

# The coexistence of Majorana fermion and Jackiw-Rebbi-type bound state, a legend of half fermion and half fermion parity

Ye Xiong

*Department of Physics and Institute of Theoretical Physics ,  
Nanjing Normal University, Nanjing 210023, P. R. China\**

Peiqing Tong

*Department of Physics and Institute of Theoretical Physics ,  
Nanjing Normal University, Nanjing 210046, P. R. China  
Jiangsu Key Laboratory for Numerical Simulation of Large Scale Complex Systems,  
Nanjing Normal University, Nanjing 210023, P. R. China and  
Kavli Institute for Theoretical Physics China, CAS, Beijing 100190, China†*

We find the coexistence of two kinds of non-abelian quasiparticles, Majorana fermion and Jackiw-Rebbi-type bound state (JRBS), in one-dimensional (1D) system in a topological superconducting phase. Unlike that in the absence of superconducting pairing, the fractional charge carried by each JRBS is not the universal one  $e/2$  in general. This is because the BdG superconductivity breaks particle number conservation. As the parity of fermion numbers is still conserved, the sharp observable carried by each JRBS is half parity, instead of the half elemental charge. We propose two different 1D models and a topological argument, as well as a numerical calculation, to illustrate the fractional parity carried by each JRBS.

PACS numbers: 73.63.Nm, 74.45.+c, 14.80.Va, 75.60.Ch

*Introduction.*— It has been proposed that Majorana Fermions (MF) can exist at the core of magnetic vortex penetrating a 2-dimensional (2D)  $p_x \pm ip_y$  superconductor[1–7] or at the end of a 1-dimensional (1D)  $p$  wave superconductor [5, 8–12]. These MFs, being their own anti-particles, obey non-abelian braiding statistics so that the quantum computing based on them is fault-tolerant [3, 13]. Beside MF, Jackiw-Rebbi-type bound states (JRBS) [14] carrying fractional charge(FC)  $e/2$  at a domain-wall (or at the ends) are also interesting because they also obey non-abelian braiding statistics[15].

Unlike FC excitations in many-body problems, such as quarks, excitations in the fractional quantum Hall (or fractional topological) system and excitations in 1D Luttinger liquid[3, 16–19], JRBS is well understood within a single particle scenario. It was found that the bound states at domain-wall (or end) in the spinful Su-Schrieffer-Heeger (SSH) model [10, 20–22] were JRBSs. But the wall does not carry FC in that case because it triggers two spin-degenerate JRBSs. These two JRBSs will induce spin-charge separation on the domain-wall but compensate the FC carried by each individual JRBS[10, 23]. To find a domain-wall with FC, one needs to include spin-orbital interaction and a magnetic field [24, 25] or a rotating magnetic field [11] to lift the spin degeneracy and tune models so that the domain-wall can only trigger JRBS in one spin direction but not in the other direction.

In Ref. [11], it is found that in Rashba nanowire the bound states at the ends can change from JRBS to MF, accompanied with a topological phase transitions in bulk.

In this letter, we show that JRBS can coexist with MF in a new topological superconducting phase (TSP), that emerges only in dimerized 1D models. In this phase, MFs are bounded at the ends, at the same time JRBS can appear at domain-wall. This exotic behavior can be well understood by decoupling model into two partial spinless Hamiltonians, one with  $p$  wave superconducting pairing [1, 26] that sustaining MF bound states and the other being an insulator that supporting JRBS. As domain-wall can only trigger one JRBS, it should carry FC. In this case, two kinds of non-abelian quasi-particles in 1D system can be integrated together and their braidings should be interesting.

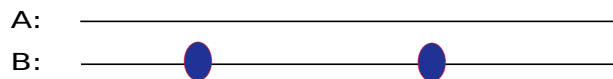


FIG. 1: A schematic indicating the effect of JRBS. The chains  $A$  and  $B$  are identical elsewhere except that  $B$  has two long separate JRBSs.

We use two dimerized models to illustrate our conclusions, one stems from SSH model and the other is a lattice model with local anti-ferromagnetic (AF) order. The domain-walls are, like those in the SSH model, produced by distorting the perfect staggered lattice with two adjacent stronger or weaker bonds in the former model and AF domain-wall in the latter one. We find that both kinds of domain-walls bring FC JRBS. But because the presence of Bogoliubov-de Gennes (BdG) superconducting pairing breaks fermion number conservation, charge as well as FC are not sharp quantum observables. The JRBS in this case is carrying fractional parity (FP) of

particle number indeed. We illustrate this in a schematic in Fig. 1 with two long chains, denoted as A and B respectively. The only difference between them is that B has a pair of JRBSs. These JRBSs are longly separated so that each one can be considered individually. In the absence of superconducting pairing,  $\Delta = 0$ , the total numbers of fermions on these chains are well defined, denoted as  $N_A$  and  $N_B$  respectively. We will show that  $|N_A - N_B| = 1$ . So each JRBS takes the responsibility of the half of this particle number difference, which leads to FC  $e/2$ . But when the superconducting pairing  $\Delta$  is tuned on, the conserved quantities on A and B regress from particle numbers to parities of numbers,  $P_{A(B)} = N_{A(B)} \bmod 2$ . The well defined (conserved) quantities on A and B are different by  $|P_A - P_B| = 1$ . In this sense, each JRBS will indeed takes the responsibility of the half of fermion parity. The actual electric charge  $Q$  carried by each JRBS is not a universal value,  $e/2$ , anymore.

*The model for cold fermions.*—We start from an effective Hamiltonian for a 1D spinful topological superfluid model

$$\begin{aligned}
H = & \sum_{i\beta} \mu c_{i\beta}^\dagger c_{i\beta} + \sum_{i\beta\gamma} [1 - (-1)^i \delta] c_{i+1\beta}^\dagger \sigma_{\beta\gamma}^z c_{i\gamma} \\
& + \sum_{i\beta\gamma} B c_{i\beta}^\dagger \sigma_{\beta\gamma}^z c_{i\gamma} + \alpha_R \sum_i (c_{i\uparrow}^\dagger c_{i+1\downarrow} - c_{i\downarrow}^\dagger c_{i+1\uparrow}) \\
& + \sum_i \Delta c_{i\uparrow}^\dagger c_{i\downarrow}^\dagger + \text{h.c.} \quad (1)
\end{aligned}$$

Here,  $c_{i\beta}$  and  $c_{i\beta}^\dagger$  are the annihilation and creation operators for spinful fermion with spin  $\beta$  on site  $i$  and  $\sigma$ 's are Pauli matrices. The energy units are set as the uniform part of hopping. The parameters  $\mu$ ,  $\delta$ ,  $\alpha_R$  and  $\Delta$  are for the chemical potential, the staggered part of hopping, the spin-orbital interaction and the superconducting pairing, respectively.

As showed in the Supplemental Material [27], this effective Hamiltonian is describing cold fermions on a 1D lattice with staggered hopping [28, 29], staggered spin-orbital interaction [4] and Fulde-Ferrell (FF) superconducting pairing. The FF pairing with finite momentum for the centers of Cooper pairs is spontaneously induced in 1D cold atoms with spin-orbital interaction at low temperature [30–33]. So one only needs to generate the staggered hopping and the staggered spin-orbital terms, which have been realized or proposed to be realized, to simulate the model in cold fermions.

The detailed phase diagram has been given in the Supplemental Material [27]. Here we only show two typical energy spectrum. In Fig. 2(a), we plot energy spectrum for Hamiltonian Eq. 1 with open boundary condition. The length of the chain is  $N = 400$  and the chemical potential is  $\mu = 0$ . There is one zero energy bound state in the band gap in two regions: region I in  $0.05 < |B| < 0.65$  and region II in  $1.7 < |B| < 2.3$ . These regions are

caused by different factors. As the border of region II indicates[27], it stems from the superconducting proximity effect around the quantum critical point  $|B| = 2$  at which the band gap closes in the non-superconducting model. It exists in the absence of staggered part of hopping and has been well studied. Region I is a new one induced by the staggered hopping because it appears only when  $\delta > \alpha_R$ . In the Supplemental Material [27], the above two regions are confirmed to be in TSP by a topological invariant.

As Fig. 2(a) shows, there is also another exotic region in  $0.65 < |B| < 1.7$ . Two zero energy bound states appear. Erikas *et. al.* have discussed the Kramers MF bound states in a two-chains model with particle-hole and time-reversal symmetry in Ref. [34]. The two zero-energy bound states in our model are similar to the Kramers MF pair but the time-reversal symmetry has been replaced by the sublattice symmetry when  $\mu = 0$ .

In Fig. 2(b), we plot the energy spectrum for the model with periodic boundary condition and the length of ring is changed to  $N = 401$ . As the length of the unit cell is 2, the ring contains insuppressible half unit cell. So this ring naturally engages a domain-wall and the energy spectrum exhibits bound states near it. In Fig. 2(b) MF zero energy state disappears as there is no geometric end. Outside region I, the energies of bound states are adjacent to the bulk band, implying that the domain-wall can only be considered as a normal impurity. In region I, however, a bound state deep in gap can evolve continuously crossing the zero energy. This implies that domain-wall in region I should be considered as a topological impurity that triggers *one* JRBS.

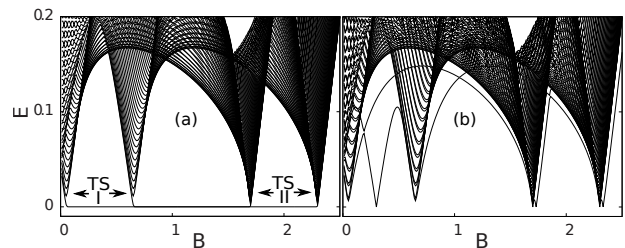


FIG. 2: The energy spectrum for  $N = 400$  chain with open boundary condition (a) and for  $N = 401$  ring with periodic boundary condition (b). Parameters are  $\delta = 0.2$ ,  $\Delta = 0.3$ ,  $\alpha_R = 0.1$  and  $\mu = 0$ . In (a), a single zero energy state appears in two regions: region I  $0.05 < |B| < 0.65$  and region II  $1.7 < |B| < 2.3$ . There are two zero energy bound states in the region  $0.65 < |B| < 1.7$ . Panel (b) shows that a domain-wall can bring *one* bound state deep in band gap in region I.

*Numerical calculation of electric charge carried by a domain-wall.*— In Fig. 3, we numerically calculate the total electric charge  $Q$  (in the units of  $e$ ) carried by a domain-wall. As defined in the SSH model[22], we let

$$Q = \rho_L^{\text{WD}} - \rho_L^0, \quad (2)$$

where  $\rho_L^{\text{WD}}$  is the total particle number in a segment with a domain-wall at its center and  $\rho_L^0$  is the particle number for a segment without domain-wall.  $L$  is the length of these segments that should exceed the localization length of the JRBS. In the numerical calculation, we choose  $L = 200$  which is long enough to find the saturated  $Q$ .

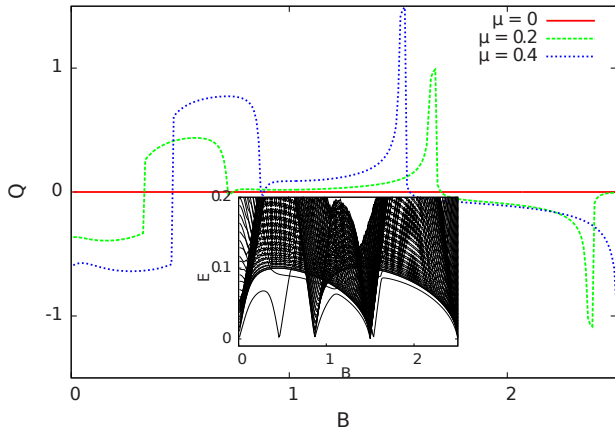


FIG. 3: Electric charge carried by a domain-wall. The system is the same as that in panel (b) of Fig. 2.  $\rho_L^{\text{WD}}$  and  $\rho_L^0$  are numerically calculated in the two parts of the ring, with a domain-wall at the center and far away from the domain-wall, respectively. The lengths of the two parts are  $L = 200$ . The inset shows the energy spectrum for the model with  $\mu = 0.4$ .

Fig. 3 shows that, when  $\mu = 0$ , the domain-wall is neutral in all phases. This is because the particle number on each site is exactly one, independent of the presence of domain-wall. But when we switch on chemical potential  $\mu$ , in region I the wall carries decimal charge. The absolute value of the charge increases with  $\mu$ . There is also a sign switch near the center of region I. This switch is caused by the particle hole transition for the bound state that is showed as a zero energy crossing in Fig. 2(b). In inset, we show the energy spectrum for a ring with  $\mu = 0.4$ . The spectrum shows that the phase diagram is not modified dramatically by increasing  $\mu$ . It ensures us to keep using the phase specifications in the  $\mu = 0$  case. For region II, the charge shows a peak and a dip at the phase boundaries. But it is almost zero inside the region. We suggest that the peak and dip are due to the quantum fluctuation accompanied with the band gap closing.

So we find that the electric charge carried by a domain-wall is decimal in region I. This charge is not universal  $e/2$  and depends on the parameters. Actually, the charge or the particle number is not well defined in a BdG superconductor. In this sense, the electric charge we just numerically obtained is not a sharp quantum observable. This situation is different from that in Refs. [14, 15, 23–25], where in the absence of BdG superconducting coupling particle number is a conserved quantum number. We will use a topological picture to illustrate that JRBS is actually carrying *fractional parity*, where the parity of

particle numbers, rather than the charge, is a sharp (conserved) quantum observable in a BdG superconductor.

*Fractional parity JRBS.*— We first study the evolution of Wannier functions(WF) during Thouless pump. These evolutions not only illustrate the topology of the band structure in the Brillouin zone, but also help us specify the nature of JRBS.

The extended Thouless pump to our spinful model is introduced by modifying the Hamiltonian with an extra parameter  $\phi$ ,  $H(\phi) = H_0(\phi) + H_{\text{st}}(\phi)$ , where  $H_{\text{st}}(\phi) = \sum_i h_{\text{st}} \sin(\phi) (-1)^i (c_{i\uparrow}^\dagger c_{i\uparrow} - c_{i\downarrow}^\dagger c_{i\downarrow})$  and  $H_0(\phi)$  is the modified Hamiltonian by replacing  $\delta$  with  $\delta \cos(\phi)$  in Eq. 1. The absolute value of  $h_{\text{st}}$  is moderate so that the band gap at the Fermi energy is not closed during the pump.

The most localized WFs [35–37] for the occupied bands are obtained from the eigenvectors of the tilde position operator  $\tilde{R}(\phi) = \hat{P}(\phi)\hat{R}\hat{P}(\phi)$ , where  $\hat{R}$  is the position operator extended to the Nambu representation and  $\hat{P}(\phi)$  is the project operator on the occupied states ( $E < 0$ ) for the Hamiltonian  $H(\phi)$ . Here the position operator is  $\hat{R} = \text{diag}(1, 2, \dots, N)\tau_0$ , where  $\tau_0$  is the  $2 \times 2$  unit matrix in the particle-hole subspace and  $\text{diag}(1, 2, \dots, N)$  is a diagonal matrix with the diagonal elements running through lattice sites from 1 to  $N$ . The project operator is  $\hat{P}(\phi) = \sum_{\alpha \in \text{occupied states}} |\alpha(\phi)\rangle\langle\alpha(\phi)|$ . The eigenvalues of  $\tilde{R}$ , denoted as  $R_s$ , are the central positions of the WFs.

In Fig. 4, we plot the energy spectrum (a) and the centers of WFs (b) during the Thouless pump with the parameters in region I. The energy spectrum shows that with the moderate value of  $h_{\text{st}} = 0.3$ , the band gap keeps open during the pump. This fact ensures that the WFs are localized and their centers showed in (b) are reliable.

In Fig. 4(b), the centers of WFs during the pump are showed. According to their evolution, these WFs can be classified into two groups, one corresponding to the WFs that do not change their position after a circle of pump and the other corresponding to the WFs that change their positions by one unit cell. The WFs in the latter group can be further divided into two kinds, one (in blue) is those moving in the positive direction with  $\phi$  and the other (in red) includes those moving inversely. In the Supplemental Material [27], we show that the above two groups of WFs inherit the properties from those of the partial Hamiltonians  $H_{\pm}$ , respectively. With the parameters in Fig. 4, the Thouless pump will induce a trival evolution for the WFs (WFs come back to their initial positions after a circle of pump) from  $H_+$ . But the evolution of WFs from  $H_-$  is nontrivial (WFs switch one unit cell after the circle). If transferring  $H_{\pm}$  back to the lattice representation through an inverse Fourier transformation, one can find MF in  $H_+$  while JRBS in  $H_-$ . We have also studied the evolution of WFs with the parameters in region II. But the WFs do not show any nontrivial evolution in that case.

Fig. 4(b) helps us recognize that each JRBS carries FP. The proof includes several steps and we would like to highlight the goal of each step first. In the 1st step, besides chains A and B showed in Fig. 1, an auxiliary chain C is employed. C is not uniform but with the Thouless pump parameter  $\phi$  varying slowly along the chain from 0 to  $2\pi$ . The other parameters are the same as those in the uniform chain A. From the evolution of WFs showed in Fig. 4 (b), we can conclude that C and A are only different by one pair of WFs. In the 2nd step, we prove that B and C have same number of WFs. In this sense, through the bridge built by C, we find that A and B are different by the pair of WFs. In the 3rd step, at a particular set of parameters,  $\mu = 0$ ,  $B = 0.3$  and  $\alpha_R = 0$ , the difference of the pair of WFs implies that the total number of quasi-particles in A and B are different by one in the mixed representation of  $H_{\pm}$ . In the 4th step, after coming back to the original Nambu representation, the above one quasi-particle difference is equivalent to parity difference between A and B. When the parameters leave away from the particular ones, the above conclusion is not modified as long as they are still in region I. In the 5th step, this conclusion is numerically proved through a direct calculation of parity of fermion numbers in A and B.

*The first step.*— Let us compare the positions of WFs in two infinite chains A and C, one is a uniform chain with  $\phi = 0$  and the other is a chain on which  $\phi$  is slowly varying  $2\pi$  along it. Without loss of generality, we let  $\phi(-\infty) = 0$  and  $\phi(+\infty) = 2\pi$  in C. Because  $\phi(x)$  is varying very slowly, in each macroscopically small but microscopically large segments, it can be considered as a constant. This ensures us to find the positions of the WFs in each segment in the latter chain. For the segments at  $x = -\infty$ , the positions of WFs in two chains are identical. But as  $x$  is increasing, compared with those in A, a set of WFs (in blue) in C begins to misalign slightly in the positive  $x$  direction while another set of WFs (in red) has misaligned simultaneously in the negative direction. As we sweeping our focus through the chains from  $x = -\infty$  to  $x = +\infty$ , the above misalignments increase and finally reach  $\pm 2$ , the length of a unit cell. This can be considered as that tuning on  $\phi(x)$  adiabatically will push a WF (in blue) outside and pull a WF (in red) in at  $x = +\infty$ . So we can conclude that compared with the uniform chain, C donates one WF (in blue) and accepts another WF (in red).

*The second step.*— Now we relax the restriction that  $\phi(x)$  is varying slowly along C. This relaxation does not affect the above conclusion because local fluctuations of  $\phi(x)$  can not distort the global property happening at  $x = +\infty$ . For simplicity, we let  $\phi(x)$  jumps  $\pi$  at two long separate points and keeps constant elsewhere. This new layout of  $\phi(x)$  is just describing a chain with a pair of domain-walls, which has been schematically showed in Fig. 1 as chain B. So this pair of domain-walls must take

the responsibility of the pair of WFs that have been lost and gained. Because the two domain-walls are identical through a mirror reflection, their properties must be the same. So each domain-wall is in response to *one half* of the WF pair.

*The third step.*— With the particular parameters,  $\mu = 0$ ,  $\delta = 0.2$ ,  $\Delta = 0.3$ ,  $B = 0.3$  and  $\alpha_R = 0$ , the Hamiltonian  $H(k)$  can be decoupled into two parts,  $H_{\pm}$ . As showed in the Supplemental Material [27], the pair of WFs that have been lost and gained comes from those of  $H_-$ . So we only need to focus on the partial Hamiltonian  $H_-$ , which has been given explicitly [27]. In this representation,  $\alpha_R$  is playing the role of superconducting pairing in this partner Hamiltonian. When  $\alpha_R = 0$ , this Hamiltonian regresses to a standard spinless SSH model. The dimension of  $H_-$  has been extended from that of the standard spinless SSH model,  $2 \times 2$ , to  $4 \times 4$  because a Nambu representation is still taken. The two sets of WFs, in blue and in red, come from the empty conduction band and the filled valence band of the SSH model, respectively [38]. So in the representation of  $H_-$ , the pair of lost and gained WFs corresponds to one quasi-particle difference.

*The fourth step.*— After returning back to the ordinal Nambu representation of  $H(k)$ , the one quasi-particle difference between A and B corresponds to the difference of the parities of fermion numbers in A and B. Tuning on  $\alpha_R$  and  $\mu$  does not disturb this conclusion because the spin-orbital interaction and chemical potential commute with particle number operator so that they also commute with the parity. As each JRBS takes the responsibility of half of this parity difference, we conclude that it carries FP in the presence of superconducting pairing.

*The fifth step.*— We have proved that the parity of fermion numbers in A and B are different. This can be confirmed numerically by calculating the number parity of A and B directly. The length of the chains are decreased from  $N = \infty$  to  $N = 400$  and a periodic boundary condition has been employed to eliminate boundary effect. The parity of fermion numbers of a ring can be calculated by  $P = \text{rank}(v) \bmod 2$  [39], where  $\text{rank}(v)$  is the rank of Bogoliubov matrix  $v$ . We find  $|P_A - P_B| = 1$  in region I and  $|P_A - P_B| = 0$  elsewhere.

*Another model with local AF order.*— We also investigate another model with uniform hopping, uniform spin-orbital interaction and uniform  $s$  wave superconducting pairing. The crucial term is the local AF magnetic order. We find that JRBS carrying FP can also coexist with MFs. The detailed discussion is put in the Supplemental Material [27].

*Conclusions.*— We have showed that JRBS and MF can coexist in a TSP in 1D models. As the presence of superconducting pairing breaks particle number conservation, the electric charge attached to each JRBS is not universal,  $e/2$ . Instead, the universal value should be referred to one half of the parity of particle number.

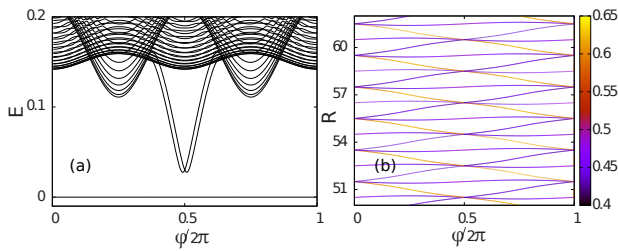


FIG. 4: The energy spectrum for  $H(\phi)$  with open boundary condition (a) and the associated centers of WFs (b). The length of chain is  $N = 400$ . Parameters are  $\delta = 0.2$ ,  $\Delta = 0.3$ ,  $\mu = 0.1$ ,  $\alpha_R = 0.1$  and  $h_{st} = 0.3$ . The color palette in (b) is indicating the weights of WFs projected onto the particle subspace in Nambu representation.

We have proposed two models, which may be realized with cold atoms and semiconductor heterostructure respectively, that can host these two kinds of topological impurities obeying non-abelian braiding statistics. We believe the integration of these two impurities can enrich the quantum implements on the information storied in them. For instance, we have showed that, in a spinless model, one can apply a NOT operation on the MF qubit by moving a JRBS adiabatically around a ring [38]. It still remains challenging how to experimentally observe the FP JRBS. One possible way is the proposal in Ref. [24]. The  $4\pi$  period is still the sign of FP JRBS although the electric charge is not  $e/2$  in this case.

*Acknowledgments.*— The work was supported by the State Key Program for Basic Research of China (Grant Nos. 2009CB929504, 2009CB929501), National Foundation of Natural Science in China Grant Nos. 10704040, 11175087.

\* Electronic address: xiongye@njnu.edu.cn

† Electronic address: pqtong@njnu.edu.cn

- [1] D. a. Ivanov, Phys. Rev. Lett. **86**, 268 (2001), ISSN 0031-9007.
- [2] X.-L. Qi and S.-C. Zhang, Rev. Mod. Phys. **83**, 1057 (2011).
- [3] C. Nayak, S. H. Simon, A. Stern, M. Freedman, and S. Das Sarma, Rev. Mod. Phys. **80**, 1083 (2008).
- [4] X.-J. Liu, T. Law, K., and K. Ng, T., Phys. Rev. Lett. **112**, 086401 (2014).
- [5] L. Fu and C. L. Kane, Phys. Rev. Lett. **100**, 096407 (2008).
- [6] X.-L. Qi, T. L. Hughes, and S.-C. Zhang, Phys. Rev. B **82**, 184516 (2010).
- [7] X.-W. Yan, M. Gao, Z.-Y. Lu, and T. Xiang, Phys. Rev. B **84**, 054502 (2011).
- [8] A. Y. Kitaev, Phys. Usp. **44**, 131 (2001).
- [9] J. D. Sau, R. M. Lutchyn, S. Tewari, and S. Das Sarma, Phys. Rev. Lett. **104**, 040502 (2010).
- [10] S.-Q. Shen, *Topological Insulators, Dirac Equation in Condensed Matters* (Springer Series in Solid-State Science 174, 2012).
- [11] J. Klinovaja, P. Stano, and D. Loss, Phys. Rev. Lett. **109**, 236801 (2012).
- [12] A. C. Potter and P. A. Lee, Phys. Rev. Lett. **105**, 227003 (2010).
- [13] M. Z. Hasan and C. L. Kane, Rev. Mod. Phys. **82**, 3045 (2010).
- [14] R. Jackiw and C. Rebbi, Phys. Rev. D **13**, 3398 (1976).
- [15] J. Klinovaja and D. Loss, Phys. Rev. Lett. **110**, 126402 (2013).
- [16] F. Wilczek, *Fractional Statistics and Anyon Superconductivity* (World Scientific, Singapore, 1990).
- [17] N. H. Lindner, E. Berg, G. Refael, and A. Stern, Phys. Rev. X **2**, 041002 (2012).
- [18] A. Vaezi, Phys. Rev. B **87**, 035132 (2013).
- [19] Y. Oreg, E. Sela, and A. Stern, Phys. Rev. B **89**, 115402 (2014).
- [20] W. P. Su, J. R. Schrieffer, and A. J. Heeger, Phys. Rev. Lett. **42**, 1698 (1979).
- [21] W. P. Su, J. R. Schrieffer, and A. J. Heeger, Phys. Rev. B **22**, 2099 (1980).
- [22] S. Kivelson and J. R. Schrieffer, Phys. Rev. B **25**, 6447 (1982).
- [23] S. Gangadharaiyah, L. Trifunovic, and D. Loss, Phys. Rev. Lett. **108**, 136803 (2012).
- [24] D. Rainis, A. Saha, J. Klinovaja, L. Trifunovic, and D. Loss, Phys. Rev. Lett. **112**, 196803 (2014).
- [25] J. I. Väyrynen and T. Ojanen, Phys. Rev. Lett. **107**, 166804 (2011).
- [26] J. J. He, K. Ng, T., P. A. Lee, and T. Law, K., Phys. Rev. Lett. **112**, 037001 (2014).
- [27] See *Supplemental Material* (????).
- [28] J. P. Hague and C. MacCormick, New J. of Phys. **14**, 033019 (2012).
- [29] M. Atala and et. al., arXiv:1212.0572 (2012).
- [30] H. Lu, L. O. Baksmaty, C. J. Bolech, and H. Pu, Phys. Rev. Lett. **108**, 225302 (2012).
- [31] Y. Xu, R.-L. Chu, and C. Zhang, Phys. Rev. Lett. **112**, 136402 (2014).
- [32] P. Fulde and R. A. Ferrell, Phys. Rev. **135**, A550 (1964).
- [33] C. Chen, Phys. Rev. Lett. **111**, 235302 (2013).
- [34] E. Gaidamauskas, J. Paaske, and K. Flensberg, Phys. Rev. Lett. **112**, 126402 (2014).
- [35] D. Thouless, J. Phys. C **17**, L325 (1984).
- [36] T. Thonhauser and D. Vanderbilt, Phys. Rev. B **74**, 235111 (2006).
- [37] X.-L. Qi, Phys. Rev. Lett. **107**, 126803 (2011).
- [38] X. Ye and T. Peiqing, arXiv:1406:5568 (2014).
- [39] G. Ben-Shach, A. Haim, I. Appelbaum, Y. Oreg, A. Yacoby, and B. I. Halperin, arXiv:1406:5172 (2014).

# The coexistence of Majorana fermion and Jackiw-Rebbi-type bound state, a legend of half fermion and half fermion parity

Ye Xiong P. Q. Tong

PACS numbers:

arXiv:1407.3532v1 [cond-mat.str-el] 14 Jul 2014

## I. THE SYSTEM OF THE FIRST HAMILTONIAN.

We are considering cold fermions trapped in a 1D laser induced lattice. The staggered hoppings like that in the SSH model has been realized in the experiment<sup>1,2</sup>. In a recent proposal<sup>3</sup>, the staggered effective spin-orbital interaction can also be produced with the aid of modern technologies. It was known that the spin-orbital coupled Fermi gas is dominated by Fulde-Ferrell (FF) superfluid phase in 1D models at low temperature. In this paper, we simulate the FF phase with a stagger pairing coefficient. So the Hamiltonian reads

$$H = \sum_{i\beta} \mu c_{i\beta}^\dagger c_{i\beta} + \sum_{i\beta} (1 - (-1)^i \delta) c_{i\beta}^\dagger c_{i+1\beta} + \sum_{i\beta\gamma} B c_{i\beta}^\dagger \sigma_{\beta\gamma}^z c_{i\gamma} - \sum_i (-1)^i \alpha_R (c_{i\uparrow}^\dagger c_{i+1\downarrow} + c_{i\downarrow}^\dagger c_{i+1\uparrow}) + \sum_i (-1)^i \Delta c_{i\uparrow}^\dagger c_{i\downarrow}^\dagger + \text{h.c.}, \quad (1)$$

where chemical potential, staggered hoppings, magnetic field induced Zeeman term, staggered spin-orbital interaction and FF superfluid pairing are written, subsequently.  $\sigma$ 's are Pauli matrices and  $c_{i\beta}$  is annihilation operator on site  $i$  with spin  $\beta$ . Through a transformation on the odd lattice,  $c_{2n+1\uparrow} \rightarrow c_{2n+1\uparrow}$  and  $c_{2n+1\downarrow} \rightarrow -c_{2n+1\downarrow}$ , the staggered spin-orbital interaction is smeared out in the new representation and the Hamiltonian changes to

$$H = \sum_{i\beta} \mu c_{i\beta}^\dagger c_{i\beta} + \sum_{i\beta\gamma} (1 - (-1)^i \delta) c_{i+1\beta}^\dagger \sigma_{\beta\gamma}^z c_{i\gamma} + \sum_{i\beta\gamma} B c_{i\beta}^\dagger \sigma_{\beta\gamma}^z c_{i\gamma} + \sum_i \alpha_R (c_{i\uparrow}^\dagger c_{i+1\downarrow} - c_{i\downarrow}^\dagger c_{i+1\uparrow}) + \sum_i \Delta c_{i\uparrow}^\dagger c_{i\downarrow}^\dagger + \text{h.c.}, \quad (2)$$

which is the first Hamiltonian we studied in the letter.

## II. THE PHASE DIAGRAM OF THE FIRST MODEL.

Let's study the model with periodic boundary condition so that the wave vector  $k$  is a good quantum number. The lattice includes two sub-lattices denoted by  $A$  and  $B$  respectively. The Hamiltonian in the Hilbert space  $(\psi_{kA\uparrow}, \psi_{kB\uparrow}, \psi_{kA\downarrow}, \psi_{kB\downarrow}, \psi_{-kA\uparrow}^\dagger, \psi_{-kB\uparrow}^\dagger, \psi_{-kA\downarrow}^\dagger, \psi_{-kB\downarrow}^\dagger)^T$  reads

$$H(k) = \begin{pmatrix} H_0(k) & V(k) \\ V^\dagger(k) & -H_0(k) \end{pmatrix}, \quad (3)$$

where

$$H_0(k) = \begin{pmatrix} B & (1 + \delta) + (1 - \delta)e^{-ik} & 0 & \alpha_R(1 - e^{-ik}) \\ (1 + \delta) + (1 - \delta)e^{ik} & B & -\alpha_R(1 - e^{ik}) & 0 \\ 0 & -\alpha_R(1 - e^{-ik}) & -B & -[(1 + \delta) + (1 - \delta)e^{-ik}] \\ \alpha_R(1 - e^{ik}) & 0 & -[(1 + \delta) + (1 - \delta)e^{ik}] & -B \end{pmatrix}$$

and

$$V(k) = \begin{pmatrix} 0 & 0 & \Delta & 0 \\ 0 & 0 & 0 & \Delta \\ -\Delta & 0 & 0 & 0 \\ 0 & -\Delta & 0 & 0 \end{pmatrix}.$$

Through a unitary transformation

$$U = \frac{1}{\sqrt{2}} \begin{pmatrix} I & I \\ I & -I \end{pmatrix},$$

the Hamiltonian is transformed to

$$H(k) \rightarrow UH(k)U^{-1} = \begin{pmatrix} 0 & A(k) \\ A^\dagger(k) & 0 \end{pmatrix},$$

where  $I$  is a  $4 \times 4$  unit matrix and  $A(k) = H_0(k) + V(k)$ .

For a gapped chain, the gap should close at  $k = 0$  or  $k = \pi$  in the Brillouin zone as varying parameters. At these phase boundaries, the nonzero bulk states at the energy  $E = 0$  implies  $\det(A) = 0$ . So we have two phase boundary conditions,  $B^2 = \Delta^2 + \mu^2 + 4 \pm 4\sqrt{\Delta^2 + \mu^2}$  and  $B^2 = \Delta^2 + 4\delta^2 + \mu^2 - 4\alpha^2 \pm 4\sqrt{\Delta^2\delta^2 + \delta^2\mu^2 - \Delta^2\alpha^2}$ .

In Fig. 1, we sketch the phase diagram in  $B - \mu$ ,  $B - \alpha$ ,  $B - \Delta$  and  $B - \delta$  planes, respectively by numerically diagonalizing  $H(k)$ . The phase boundaries are consistent with the above two conditions except on the  $B$  axis when  $\alpha = 0$  or  $\Delta = 0$ . This deviation is because in these particular conditions, the model is gapless, which violates our assumption that the gap closes at  $k = 0$  or  $k = \pi$ .

A topological invariant can be defined by  $M = \frac{\Phi_{ZB}}{\pi} \text{mod } 2$ , where  $\Phi_{ZB}$  is the Zak-Berry phase integrated over the whole Brillouin zone  $\Phi_{ZB} = \int_{-\pi}^{\pi} -i\langle\psi|\partial_k|\psi\rangle dk$  and  $|\psi\rangle$  are the occupied band states. The above topological invariant specified by Zak-Berry phase is equivalent to Pfaffian invariant first introduced by Kitaev in studying 1D topological

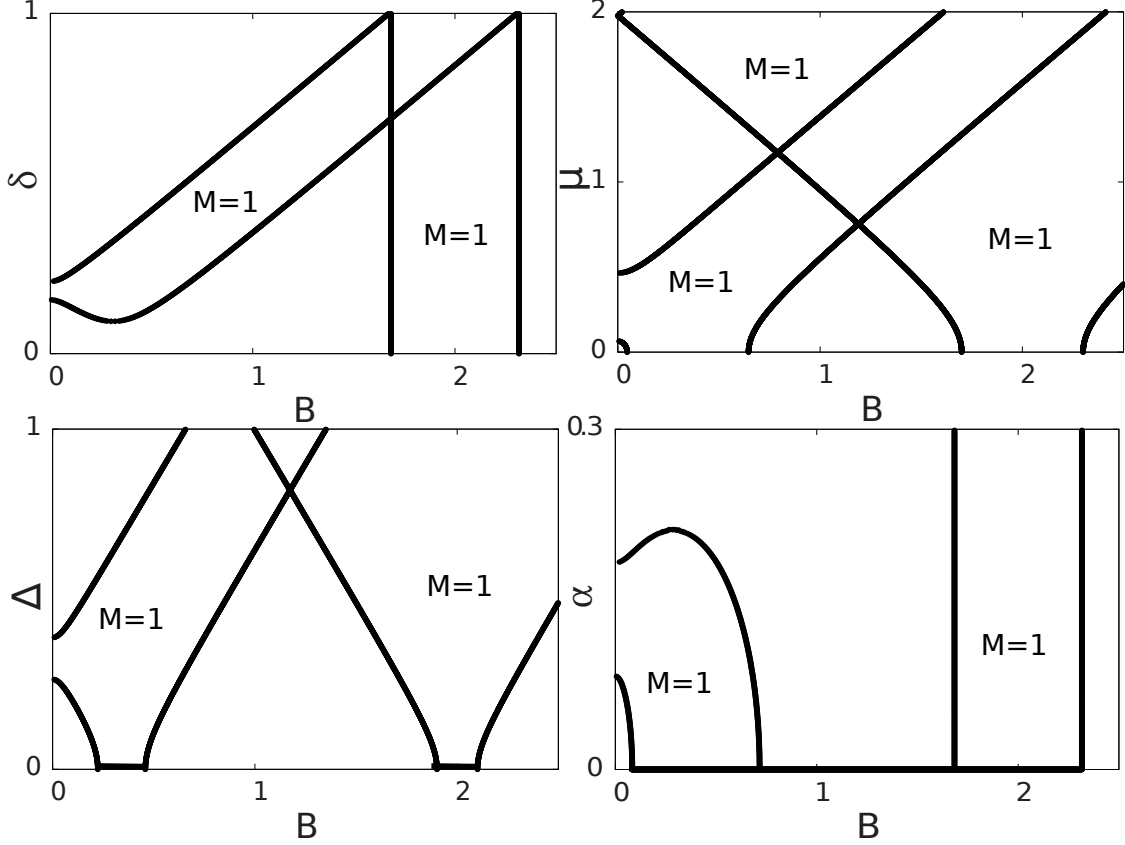


FIG. 1: The phase diagram in  $B - \delta$  (a) ,  $B - \mu$  (b),  $B - \Delta$  (c) and  $B - \alpha_R$  (d) planes. The other parameters are  $\mu = 0.1$ ,  $\alpha_R = 0.1$  and  $\Delta = 0.3$  in (a),  $\alpha_R = 0.1$ ,  $\Delta = 0.3$  and  $\delta = 0.2$  in (b),  $\alpha_R = 0.1$ ,  $\delta = 0.2$  and  $\mu = 0.1$  in (c) and  $\delta = 0.2$ ,  $\mu = 0.1$  and  $\Delta = 0.3$  in (d). The regions in TSP with topological invariant  $M = 1$  have been indicated explicitly. The rest regions are for topological trivial phase with  $M = 0$ .

superconductor<sup>4</sup>. In phase diagram Fig. 1, we indicate the regions in topological nontrivial phase with  $M = 1$ . The rest regions are for topological trivial phase with  $M = 0$ . For these topological nontrivial regions, MFs and JRBS can only coexist in region I which is a new region stemming from staggered hopping but not in region II stemming from  $B = 2$ .

To show explicitly this coexistence, we plot the energy spectrum for a open boundary chain with a domain-wall at the center. The wavefunction for the denoted bound states are showed in the representation  $(c_{i\uparrow}, c_{i\downarrow}, c_{i\uparrow}^\dagger, c_{i\downarrow}^\dagger)^T$ , where  $i$  runs through the lattice sites from 1 to  $N = 401$ . The zero energy state is bounded at the end while JRBS is bounded at the domain-wall.

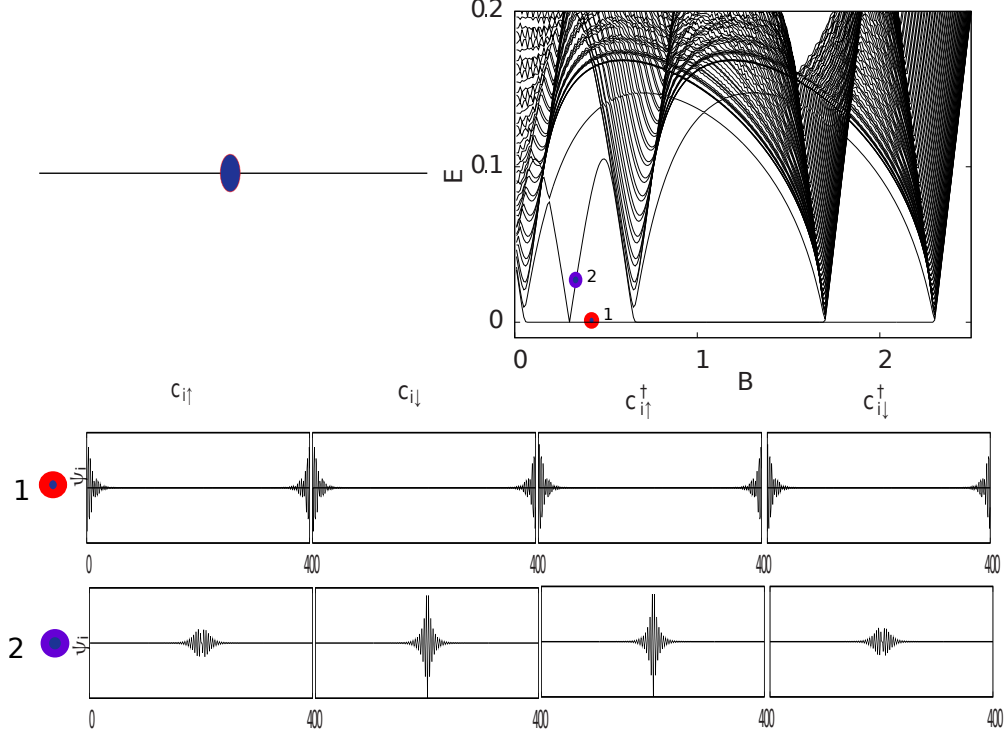


FIG. 2: Up-right corner show the energy spectrum for the chain showed in the up-left corner. The blue point in the chain is a domain-wall. The wavefunctions of MF zero energy bound state and JRBS are showed in the representation  $(c_{i\uparrow}, c_{i\downarrow}, c_{i\uparrow}^\dagger, c_{i\downarrow}^\dagger)^T$ , where  $i$  runs through the lattice sites from 1 to  $N = 401$ . The other parameters are same as those in Fig. 2 in the letter.

### III. ANOTHER WAY TO UNDERSTAND TSP WHEN $\mu = 0$ .

When  $\mu = 0$ , through a unitary transformation

$$U = \frac{1}{\sqrt{2}} \begin{pmatrix} 1 & 0 & 0 & 0 & 0 & 0 & -1 & 0 \\ 0 & 1 & 0 & 0 & 0 & 0 & 0 & -1 \\ 0 & 0 & 1 & 0 & -1 & 0 & 0 & 0 \\ 0 & 0 & 0 & 1 & 0 & -1 & 0 & 0 \\ 0 & 0 & 1 & 0 & 1 & 0 & 0 & 0 \\ 0 & 0 & 0 & 1 & 0 & 1 & 0 & 0 \\ 1 & 0 & 0 & 0 & 0 & 0 & 1 & 0 \\ 0 & 1 & 0 & 0 & 0 & 0 & 0 & 1 \end{pmatrix},$$

the Hamiltonian can be decoupled into two partitioning parts

$$H \rightarrow UHU^\dagger = \begin{pmatrix} H_+ & 0 \\ 0 & H_- \end{pmatrix}, \quad (4)$$

where

$$H_- = - \begin{pmatrix} B - \Delta & (1 + \delta) + (1 - \delta)e^{-ik} & 0 & \alpha_R(1 - e^{-ik}) \\ (1 + \delta) + (1 - \delta)e^{ik} & B - \Delta & -\alpha_R(1 - e^{ik}) & 0 \\ 0 & -\alpha_R(1 - e^{-ik}) & -B + \Delta & -[(1 + \delta) + (1 - \delta)e^{-ik}] \\ \alpha_R(1 - e^{ik}) & 0 & -[(1 + \delta) + (1 - \delta)e^{ik}] & -B + \Delta \end{pmatrix}$$

and

$$H_+ = \begin{pmatrix} B + \Delta & (1 + \delta) + (1 - \delta)e^{-ik} & 0 & \alpha_R(1 - e^{-ik}) \\ (1 + \delta) + (1 - \delta)e^{ik} & B + \Delta & -\alpha_R(1 - e^{ik}) & 0 \\ 0 & -\alpha_R(1 - e^{-ik}) & -B - \Delta & -[(1 + \delta) + (1 - \delta)e^{-ik}] \\ \alpha_R(1 - e^{ik}) & 0 & -[(1 + \delta) + (1 - \delta)e^{ik}] & -B - \Delta \end{pmatrix}.$$

We show the dispersion of the eigen-energies for the two partitioning parts,  $H_-$  and  $H_+$ , in different phases in Fig. 3, respectively. (a), (c), (e) and (g) are for  $H_-$  and (b), (d), (f), (h) are for  $H_+$ . The four rows of panels show the dispersion with  $B = 0.3$  (in region I),  $B = 1$ ,  $B = 2$  (in region II) and  $B = 2.6$ , respectively. The band inversion happens only in one part of the Hamiltonian in regions I and II. This is consistent with our conclusions in the letter that region I and II are in TSP with only one zero energy bound state. The region in between I and II can host totally two MFs, one in  $H_+$  and the other in  $H_-$ . This is because the additional sublattice symmetry changes the system class from the D to the CII<sup>5</sup> which should be characterized by a  $Z$  invariant instead of  $Z_2$  invariant.

#### IV. THE EVOLUTION OF THE CENTERS OF WANNIER FUNCTIONS DURING THOULSSS PUMP FOR THE TWO PARTIAL HAMILTONIANS.

In Fig. 4, we plot the evolution of the centers of Wannier functions during Thouless pump for the two partial Hamiltonians,  $H_+$  and  $H_-$ , respectively. If we combine the two panels together, we reproduce Fig. 4 (b) in the letter. This suggests us to separate the WFs showed in Fig. 4(b) into two groups.

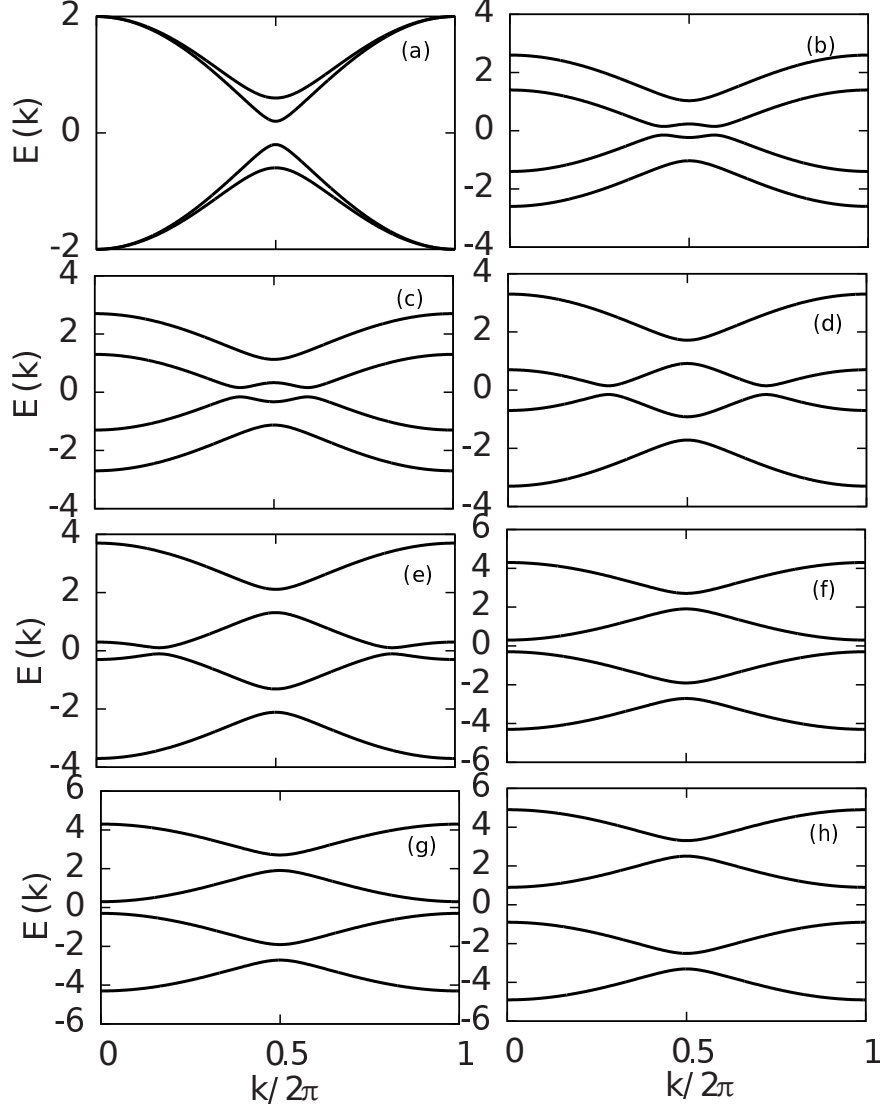


FIG. 3: The band dispersion with  $k$  for the two partial Hamiltonians,  $H_-$  (a) (c) (e) (g) and  $H_+$  (b) (d) (f) (h). The parameters are  $\alpha_R = 0.1$ ,  $\delta = 0.2$ ,  $\Delta = 0.3$  and  $B = 0.3$  (a) (b),  $B = 1$  (c) (d)  $B = 2$  (e) (f) and  $B = 2.6$  (g) (h).

## V. THE SECOND MODEL WITH LOCAL AF ORDER

The Hamiltonian reads,

$$\begin{aligned}
H = & \sum_{i\beta} [c_{i\beta}^\dagger c_{i+1\beta} + \mu c_{i\beta}^\dagger c_{i\beta}] + i\alpha_R \sum_{i\beta\gamma} c_{i\beta}^\dagger \sigma_{\beta\gamma}^y c_{i+1\gamma} \\
& + \sum_{i\beta\gamma} c_{i\beta}^\dagger (\vec{B} - \vec{M}_i) \cdot \vec{\sigma}_{\beta\gamma} c_{i\gamma} + \sum_i \Delta c_{i\uparrow}^\dagger c_{i\downarrow}^\dagger + \text{h.c.},
\end{aligned} \tag{5}$$

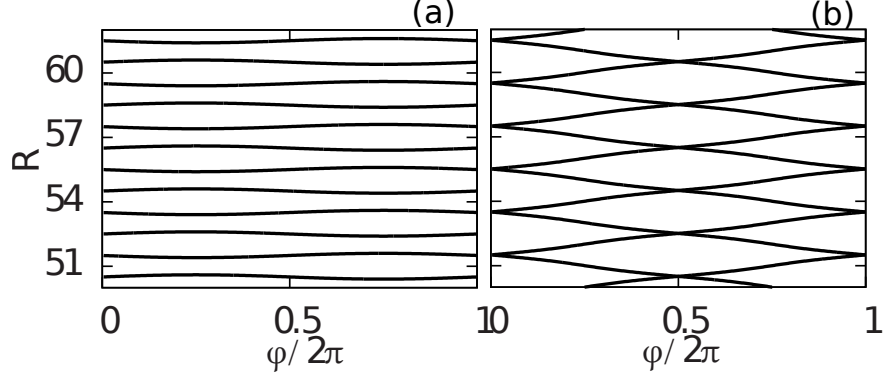


FIG. 4: The evolution of the centers of Wannier functions during Thouless pump for the two partial Hamiltonians,  $H_+$  (a) and  $H_-$  (b). The parameters are same as those in Fig. 4 in the letter.

where hopping, chemical potential, spin-orbital interaction, Zeeman interaction caused by a uniform magnetic field  $\vec{B}$  and staggered local magnetic momenta  $\vec{M}_i$  and s-wave superconducting pairing are expressed, respectively. We fix the magnetic field in the  $x-z$  plane with  $\vec{B} = \sin(\theta)B\hat{z} + \cos(\theta)B\hat{x}$  and the staggered local AF momenta are in the  $x$  direction,  $\vec{M}_i = (-1)^i M\hat{x}$ . In experiment, AF magnetic order and s-wave superconducting pairing can be introduced to a 1D semi-conductor through proximity effect by sandwiching it with AF material and superconductor.

This Hamiltonian in the Hilbert space  $(\psi_{kA\uparrow}, \psi_{kB\uparrow}, \psi_{kA\downarrow}, \psi_{kB\downarrow}, \psi_{-kA\uparrow}^\dagger, \psi_{-kB\uparrow}^\dagger, \psi_{-kA\downarrow}^\dagger, \psi_{-kB\downarrow}^\dagger)^T$  reads

$$H = \begin{pmatrix} H_0 & V \\ V^\dagger & -H_0 \end{pmatrix}, \quad (6)$$

where

$$H_0 = \begin{pmatrix} \mu + B \sin(\theta) & 1 + e^{-ik} & B \cos(\theta) + M & \alpha_R(1 - e^{-ik}) \\ 1 + e^{ik} & \mu + B \sin(\theta) & -\alpha_R(1 - e^{ik}) & B \cos(\theta) - M \\ B \cos(\theta) + M & -\alpha_R(1 - e^{-ik}) & \mu - B \sin(\theta) & 1 + e^{-ik} \\ \alpha_R(1 - e^{ik}) & B \cos(\theta) - M & 1 + e^{ik} & \mu - B \sin(\theta) \end{pmatrix},$$

and

$$V = \begin{pmatrix} 0 & 0 & \Delta & 0 \\ 0 & 0 & 0 & \Delta \\ -\Delta & 0 & 0 & 0 \\ 0 & -\Delta & 0 & 0 \end{pmatrix}.$$

When  $\mu = 0$ , the above Hamiltonian can also be decoupled into two partitioning parts,

$$H \rightarrow \begin{pmatrix} H_+ & 0 \\ 0 & H_- \end{pmatrix}, \quad (7)$$

where

$$H_+ = \begin{pmatrix} B \sin(\theta) + \Delta & 1 + e^{-ik} & B \cos(\theta) + M & \alpha_R(1 - e^{-ik}) \\ 1 + e^{ik} & B \sin(\theta) - \Delta & -\alpha_R(1 - e^{ik}) & B \cos(\theta) - M \\ B \cos(\theta) + M & -\alpha_R(1 - e^{-ik}) & \Delta - B \sin(\theta) & 1 + e^{-ik} \\ \alpha_R(1 - e^{ik}) & B \cos(\theta) - M & 1 + e^{ik} & -B \sin(\theta) - \Delta \end{pmatrix}$$

and  $H_- = -H_+$  after a unitary transformation

$$U = \frac{1}{\sqrt{2}} \begin{pmatrix} 1 & 0 & 0 & 0 & 0 & 0 & -1 & 0 \\ 0 & 1 & 0 & 0 & 0 & 0 & 0 & 1 \\ 0 & 0 & 1 & 0 & 1 & 0 & 0 & 0 \\ 0 & 0 & 0 & 1 & 0 & -1 & 0 & 0 \\ 0 & 0 & -1 & 0 & 1 & 0 & 0 & 0 \\ 0 & 0 & 0 & 1 & 0 & 1 & 0 & 0 \\ 1 & 0 & 0 & 0 & 0 & 0 & 1 & 0 \\ 0 & -1 & 0 & 0 & 0 & 0 & 0 & 1 \end{pmatrix}$$

So when  $\mu = 0$ , phase transition happens at the points  $M^2 = B^2 \cos(2\theta) + \Delta^2 - 4 \pm 2\sqrt{-B^4 \cos^2(\theta) \sin^2(\theta) + B^2 \Delta^2 \cos^2(\theta) + 4B^2 \sin^2(\theta) - 4\Delta^2}$  and  $M^2 = B^2 \cos(2\theta) + 4\alpha_R^2 + \Delta^2 - 2B\sqrt{-B^2 \cos^2(\theta) \sin^2(\theta) + \Delta^2 \cos^2(\theta) - 4\alpha_R^2 \sin^2(\theta)}$ . In Fig. 5, with some fixed parameters  $\theta = 0.6$ ,  $\Delta = 0.3$ ,  $\alpha_R = 0.1$ , we plot the energy dispersion with  $k$  for  $H_+$  in the first column when  $\mu = 0$  and for  $H$  in the second column when  $\mu = 0.5$ . The energy dispersion for  $H_-$  is not showed explicitly because  $H_- = -H_+$ . These panels show that unlike that in the first model, this model may be gapless when  $\mu = 0$ . So the chemical potential is crucial here to open the gap. In panel (f), we see a clear band inversion indicating that the model is in TSP.

In Fig. 6 we plot the energy spectrum for a chain with open boundary condition (left column) and for a ring with one AF domain-wall on it (right column). Like that in the first model, the AF domain-wall is simulated by two adjacent  $M_i$ s pointing to the same direction. We find in the cases (c), (d), (e) and (f), there is a TSP in which a MF zero energy bound

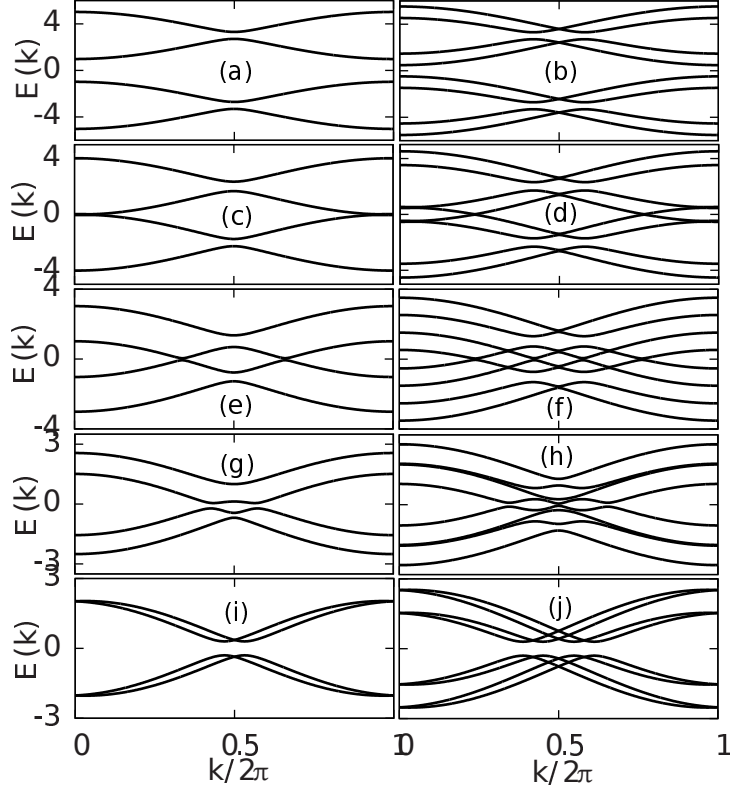


FIG. 5: The dispersion of  $H_+(k)$  (first column) and  $H(k)$  (second column). The parameters are  $\theta = 0.6$ ,  $\Delta = 0.3$  and  $\alpha_R = 0.1$  in these panels.  $B$  and  $M$  are 3 and 0 in (a) (b), 2 and 0.05 in (c) (d), 1 and 0.05 in (e) (f), 0.5 and 0.2 in (g) (h) and 0 and 0 in (i) (j).  $\mu = 0$  in (a) (c) (e) (g) (i) and  $\mu = 0.5$  in (b) (d) (f) (h) (j).

state can coexist with a JRBS. These properties are the same as those showed for the first model.

We also numerically calculate the electric charge carried by a AF domain-wall. As Fig. 7 shows, it is non-universal just as that in the first model. We also numerically calculate the parities of fermion numbers for chains like A and B. The result is same as that in the first model. So the JRBS attached to the AF domain-wall in this model is also carrying FP.

---

<sup>1</sup> J. P. Hague and C. MacCormick, New J. of Phys. **14**, 033019 (2012).

<sup>2</sup> M. Atala and et. al., arXiv:1212.0572 (2012).

<sup>3</sup> X.-J. Liu, T. Law, K., and K. Ng, T., Phys. Rev. Lett. **112**, 086401 (2014).

<sup>4</sup> J. C. Budich and E. Ardonne, Phys. Rev. B **88**, 075419 (2013).

<sup>5</sup> A. P. Schnyder, S. Ryu, A. Furusaki, and A. W. W. Ludwig, Phys. Rev. B **78**, 195125 (2008).

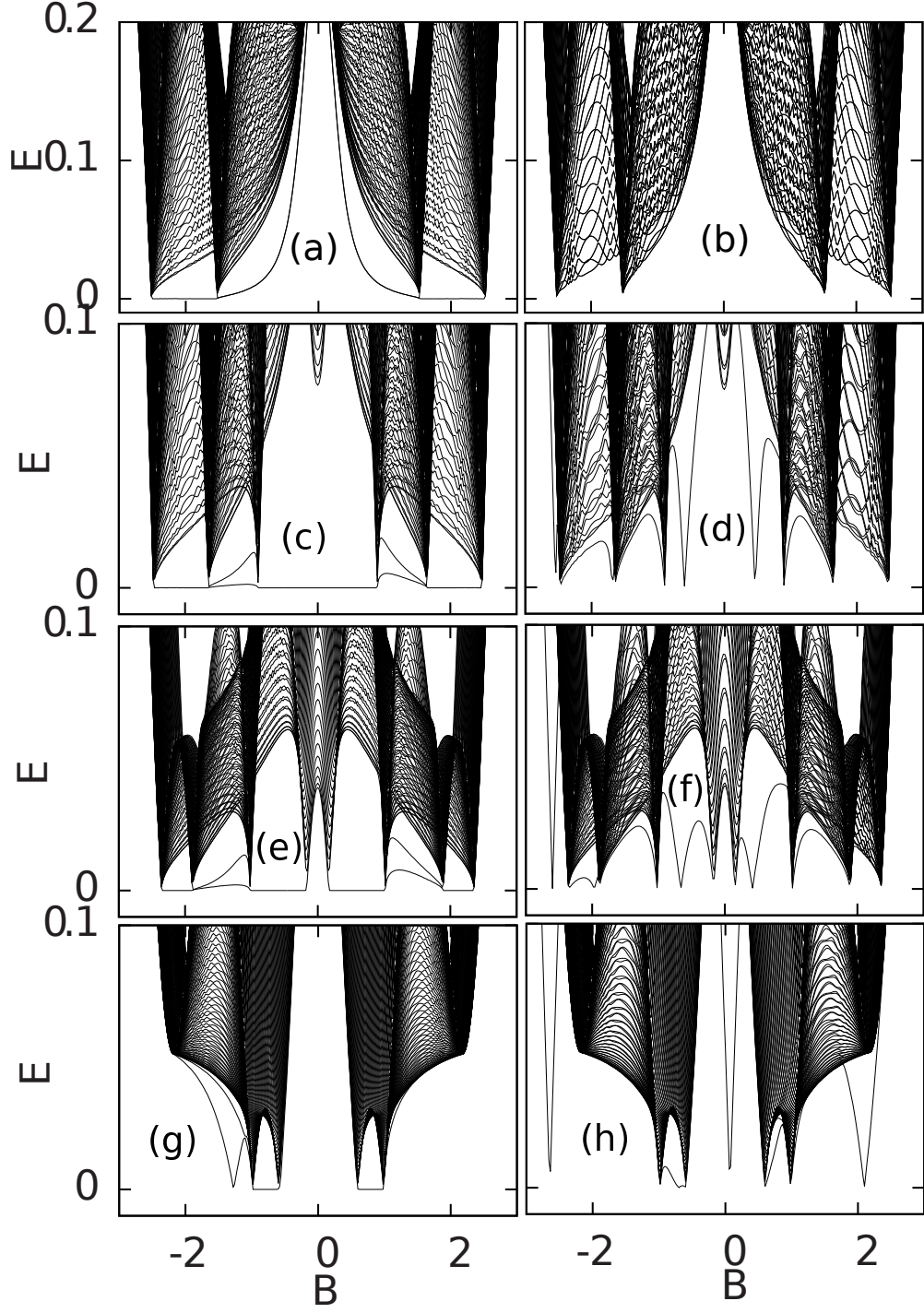


FIG. 6: The energy spectrum for a  $N = 400$  chain with open boundary condition (left column) and for a  $N = 401$  ring with a AF domain-wall (right column). The parameters are  $\theta = 0.6$ ,  $\Delta = 0.3$  and  $\alpha_R = 0.1$  in these panels.  $M$  is 0 (a) (b), 0.5 (c) (d), 0.8 (e) (f) and 1 (g) (h).

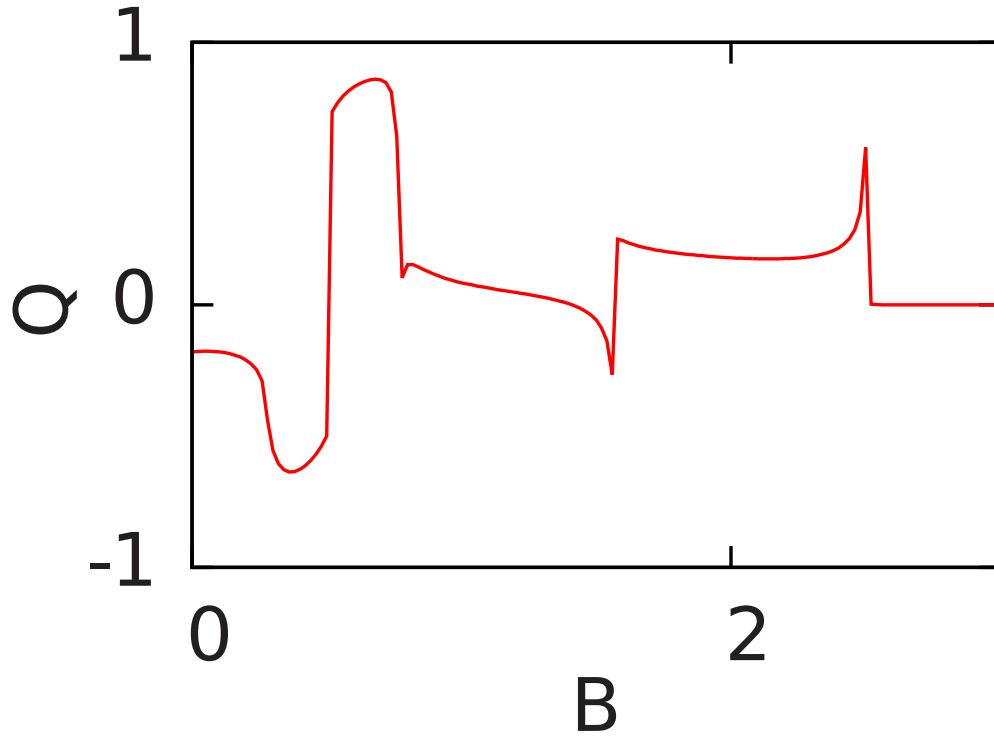


FIG. 7: The electric charge carried by a AF domain-wall. The parameters are  $\theta = 0.6$ ,  $\Delta = 0.3$ ,  $\alpha_R = 0.1$  and  $M = 0.2$ .